Synthesis, Structural Characterization, and Gas-Phase Unimolecular Reactivity of the Silver Hydride Nanocluster [Ag$_3$((PPh$_2$)$_2$CH$_2$)$_3$(μ_3-H)](BF$_4$)$_2$

Athanasios Zavras,[†,‡] George N. Khairallah,*,[†,‡] Timothy U. Connell,[†] Jonathan M. White,[†] Alison J. Edwards,[§] Roger J. Mulder,[∥] Paul S. Donnelly,*,[†] and Richard A. J. O'Hair*,[†,‡]

[†]School of Chemistry and Bio21 Molecular Science and Biotechnology Institute, University of Melbourne, 30 Flemington Road, Parkville, Victoria 3010, Australia
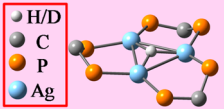
[‡]ARC Centre of Excellence for Free Radical Chemistry and Biotechnology, School of Chemistry and Bio21 Molecular Science and Biotechnology Institute, University of Melbourne, 30 Flemington Road, Parkville, Victoria 3010, Australia

[§]Bragg Institute, Australian Nuclear Science and Technology Organization, New Illawarra Road, Lucas Heights, New South Wales 2234, Australia

[∥]CSIRO Manufacturing Flagship, Bayview Avenue, Clayton, Victoria 3168, Australia

Ⓢ *Supporting Information*

ABSTRACT: A bis(diphenylphosphino)methane-ligated trinuclear silver hydride nanocluster, [Ag$_3$((Ph$_2$P)$_2$CH$_2$)$_3$(μ_3-H)](BF$_4$)$_2$, featuring three silver(I) ions coordinated to a μ_3-hydride, and its deuteride analogue, [Ag$_3$((Ph$_2$P)$_2$CH$_2$)$_3$(μ_3-D)](BF$_4$)$_2$, have been isolated and structurally characterized using electrospray ionization mass spectrometry (ESI-MS), X-ray crystallography, NMR and IR spectroscopy. The position of the deuteride in [Ag$_3$((Ph$_2$P)$_2$CH$_2$)$_3$(μ_3-D)](BF$_4$)$_2$ was determined by neutron diffraction. ESI-MS of [Ag$_3$L$_3$(μ_3-H/D)](BF$_4$)$_2$ [L = ((Ph$_2$P)$_2$CH$_2$)$_2$] produces [Ag$_3$L$_3$(μ_3-H/D)]$^{2+}$ and [Ag$_3$L$_3$(μ_3-H/D)(BF$_4$)]$^+$. A rich gas-phase ion chemistry of [Ag$_3$L$_3$(μ_3-H/D)]$^{2+}$ is observed under conditions of collision-induced dissociation (CID) and electron-capture dissociation (ECD). CID gives rise to the following complementary ion pairs: [Ag$_3$L$_2$]$^+$ and [L+(H/D)]$^+$; [Ag$_2$(H/D)L$_2$]$^+$ and [AgL]$^+$; [Ag$_2$(H/D)L]$^+$ and [AgL$_2$]$^+$. ECD gives rise to a number of dissociation channels including loss of the bis(phosphine) ligand, fragmentation of a coordinated bis(phosphine) ligand via C−P bond activation, and loss of a hydrogen (deuterium) atom with concomitant formation of [Ag$_3$L$_3$]$^+$. Under CID conditions, [Ag$_3$L$_3$(μ_3-H/D)(BF$_4$)]$^+$ fragments via ligand loss, the combined loss of a ligand and [H,B,F$_4$], and cluster fragmentation to give [Ag$_2$(BF$_4$)L$_2$]$^+$ and [Ag$_2$(L-H)L]$^+$ [where (L-H) = (Ph$_2$P)$_2$CH$^−$].

■ INTRODUCTION

Coinage metal nanoclusters (CMNCs) attract considerable attention for their fundamentally interesting structures and properties[1] and their potential for applications in areas such as catalysis,[2] medical imaging,[3] and optical materials.[4] Reports of small discrete gold nanoclusters ligated by either bis-(phosphine)[5] or thiolate ligands[6] formed via reduction of gold salts with sodium borohydride (NaBH$_4$) have appeared. Analogous reactions of silver salts with NaBH$_4$ had, in contrast, been asserted to produce silver nanoparticles instead of silver nanoclusters,[7] but reports of discrete silver nanoclusters ligated by either thiolate or a combination of thiolate and bis-(phosphine) ligands produced by analogous treatment with borohydride have since appeared. Examples include [Ag$_{14}$(SC$_6$H$_3$F$_2$)$_{12}$](PPh$_3$)$_8$;[8a] Ag$_{16}$(dppe)$_4$(SC$_6$H$_3$F$_2$)$_{14}$,[8b] and [Ag$_{32}$(dppe)$_5$(SC$_6$H$_4$CF$_3$)$_{24}$](PPh$_4$)$_2$ [dppe = 1,2-bis-(diphenylphosphino)ethane];[8b] [Ag$_{44}$(SAr)$_{30}$](PPh$_4$)$_4$ (Ar = 3,4-difluorophenyl);[9a] and M$_4$[Ag$_{44}$(p-MBA)$_{30}$] (M = alkali metal; p-MBA = p-mercaptobenzoic acid).[9b] These complexes have been carefully characterized in terms of structure and formulation, but despite the use of significant stoichiometric excess of borohydride in their synthesis, no analyses capable of excluding hydride from the formulations were reported. Instead, the prevailing assumption in CMNC chemistry that the requisite number of silver atoms are reduced to the zero oxidation state was used to yield the reported charge-balanced formula. In stark contrast, several studies of the formation and isolation of silver clusters under remarkably similar synthetic conditions have been definitively demonstrated to contain hydride ligands, and no reduction of silver in the product species was noted.[10]

As part of a program aimed at examining the gas-phase ion chemistry of bis(phosphine)-ligated CMNCs synthesized in solution and transferred to the gas phase via electrospray ionization mass spectrometry (ESI-MS),[11,12] we recently discovered that silver(I) salts in the presence of the bidentate bis(phosphine) ligand bis(diphenylphosphino)methane [dppm, (Ph$_2$P)$_2$CH$_2$, hereafter denoted as L], which were treated with NaBH$_4$, apparently produced only ligated silver(I) nanoclusters[13] rather than the mixed-valent silver(0/I) nanoclusters implicit in the compounds previously reported. The observa-

tion of abundant silver cluster ions including $[Ag_3(H)L_3]^{2+}$, $[Ag_3(H)(Cl)L_3]^+$, and $[Ag_3(Cl)_2L_3]^+$ via ESI-MS led to the synthesis, isolation, and structural characterization of $[Ag_3(\mu_3\text{-}H)(\mu_3\text{-}Cl)L_3]BF_4$ and $[Ag_3(\mu_3\text{-}Cl)_2L_3]BF_4$,[13] which has a known $[Ag_3(\mu_3\text{-}X)_2L_3]^+$ core (X = Cl, Br, I).[14] Here we report the isolation and structural characterization of the halide-free hydride-containing species $[Ag_3(\mu_3\text{-}H)L_3](BF_4)_2$ (**2**) and its deuterated analogue $[Ag_3(\mu_3\text{-}D)L_3](BF_4)_2$ (**1**). The gas-phase chemistry of $[Ag_3(H/D)L_3]^{2+}$ and $[Ag_3(H/D)(BF_4)L_3]^+$ is compared to that of $[Ag_3(H/D)(Cl)L_3]^+$ reported previously.[13]

■ RESULTS AND DISCUSSION

ESI-MS was used to monitor the types of cationic clusters present in a methanol/chloroform (1:1) solution of $AgBF_4$ and dppm at a molar ratio of 1:1 and at a concentration of 10 mM before and after the addition of 1 mol equiv of $NaBH_4$. An examination of the ESI-MS spectrum of this solution prior to the addition of $NaBH_4$ (Figure 1a) reveals the presence of
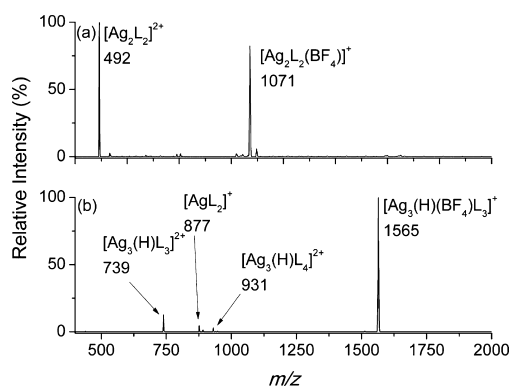

Figure 1. LTQ ESI-MS of silver clusters: (a) $AgBF_4$ and dppm in methanol/chloroform (1:1) immediately before the addition of $NaBH_4$; (b) 5 min after the addition of $NaBH_4$. The m/z values shown are of the most intense isotope peak for each given cluster or complex. Solutions containing silver clusters were diluted (50 μM) in methanol prior to ESI-MS.

abundant dinuclear complexes of dppm with silver(I), including $[Ag_2L_2]^{2+}$ (m/z 492) and $[Ag_2L_2(BF_4)]^+$ (m/z 1071). These assignments were confirmed by examination of the isotope pattern and additional high-resolution mass spectrometry (HRMS) experiments (Figure S1 in the Supporting Information, SI). The related bis(phosphine)-ligated silver(I) salts $[Ag_2L_2](NO_3)_2$ and $[Ag_2L_2](ClO_4)_2\cdot 2CH_2Cl_2$ have been structurally characterized via X-ray crystallography[16] and can be used to infer the probable structures of the $[Ag_2L_2]^{2+}$ (m/z 492) and $[Ag_2L_2(BF_4)]^+$ complexes. The silver(I) ions are bridged by the two bis(phosphine) ligands to form an eight-membered ring with approximately linear coordination at silver (with a P–Ag–P bond angle of ≈171°) and a Ag–Ag contact of ≈2.95 Å (Scheme 1).

The addition of $NaBH_4$ (or $NaBD_4$) to a methanolic solution of $AgBF_4$ and dppm results in an immediate color change from colorless to faint yellow. An aliquot of the mixture taken ca. 5 min after the addition of $NaBH_4$ was analyzed by ESI-MS, which revealed the formation of $[Ag_3(H)L_3]^{2+}$, $[AgL_2]^+$, $[Ag_3(H)L_4]^{2+}$, and $[Ag_3(H)(BF_4)L_3]^+$. The assignment of these ions was further confirmed via HRMS, which additionally showed no trace of $[Ag_2L_4]^{2+}$. The "pre-reaction phase" clusters were absent (Figure 1b), suggesting that these are consumed by the formation of $[Ag_3(H)L_3]^{2+}$ (m/z 739). As expected, the use

Scheme 1. Representation of the Cation Present in $[Ag_2L_2](ClO_4)_2$ As Determined by X-ray Crystallography Highlighting the Eight-Membered $Ag_2P_4C_2$ Ring[16a]
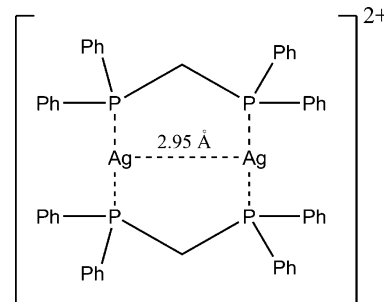
of purified chloroform in the synthesis significantly reduced the amounts of $[Ag_3(H)(Cl)L_3]^+$ (m/z 1513) and $[Ag_3(Cl)_2L_3]^+$ (m/z 1547) compared to our previous report.[13] The observation of abundant and monodisperse $[Ag_3(H/D)L_3]^{z+}(BF_4^-)_x$ {$(x, z) = (0, 2)$ and $(1, 1)$} via ESI-MS encouraged us to synthesize $[Ag_3(H)L_3](BF_4)_2$ and $[Ag_3(D)L_3](BF_4)_2$ for full characterization by ESI-MS, NMR, and IR (Figures S2−S13 in the SI).

Structural Characterization of 1 by X-ray and Neutron Diffraction. The methods developed for the ESI-MS experiments allowed us to synthesize the deuteride cluster **1** and to isolate single crystals of sufficient quality for analysis by both X-ray and neutron diffraction. The core of the cluster is composed of three silver ions forming a triangular array capped by the single deuteride (Figure 2 and Table 1). Each of the silver ions is coordinated to two phosphorus atoms and lies adjacent to the other two silver ions in a triangle, giving rise to the possibility of argentophilic interactions. The two tetrafluoroborate counterions are not coordinated to silver, but one lies in close proximity to the silver atoms and has significantly smaller displacement parameters than the less closely associated anion.

The Ag−Ag distances in $[Ag_3(\mu_3\text{-}H/D)L_3]^{2+}$ range from 3.0655(2) to 3.1511(2) Å and are markedly longer than the corresponding distances in the mixed hydride−chloride cluster $Ag_3(\mu_3\text{-}H)(\mu_3\text{-}Cl)$ (average 2.8998 Å) reported previously.[13] The deuterium atom approaches a trigonal-planar coordination mode and lies only 0.31 Å from the plane of the silver atoms, considerably closer than the 0.91 Å displacement of the hydrogen atom from the Ag_3 plane of $Ag_3(\mu_3\text{-}H)(\mu_3\text{-}Cl)$.[13] The P−Ag bond lengths range from 2.4432(4) to 2.4769(5) Å for the $[Ag_3(\mu_3\text{-}H/D)L_3]^{2+}$ cation compared to 2.4421(9)−2.4437(9) Å for $[Ag_3(\mu_3\text{-}H/D)(\mu_3\text{-}Cl)L_3]^+$. For both structures, the P−C−P bond angle in the ligand is in the range of 110.38(8)−110.52(8)°. The nearest three fluorine atoms of the closely associated BF_4^- anion, which is located on the opposite face of the Ag_3 cluster to the deuterium ligand, lie at distances of 2.695(1) (F1), 2.760 (F3), and 3.084(1) (F2) Å from the plane defined by the Ag_3 cluster, with the closest contacts being 2.841(1) (Ag2−F1), 3.082(1) (Ag1−F3), and 3.159(1) (Ag3−F4) Å. These Ag−F contacts fall within the range 2.355−3.190 Å of such contacts found from 487 observations retrieved from the Cambridge Crystallographic Database for structures of silver complexes having BF_4^- counterions.[17] It is of interest to note that the deuterium position as determined by neutron diffraction is slightly displaced toward the silver atom Ag3, which is the most weakly associated with the BF_4^- counterion.
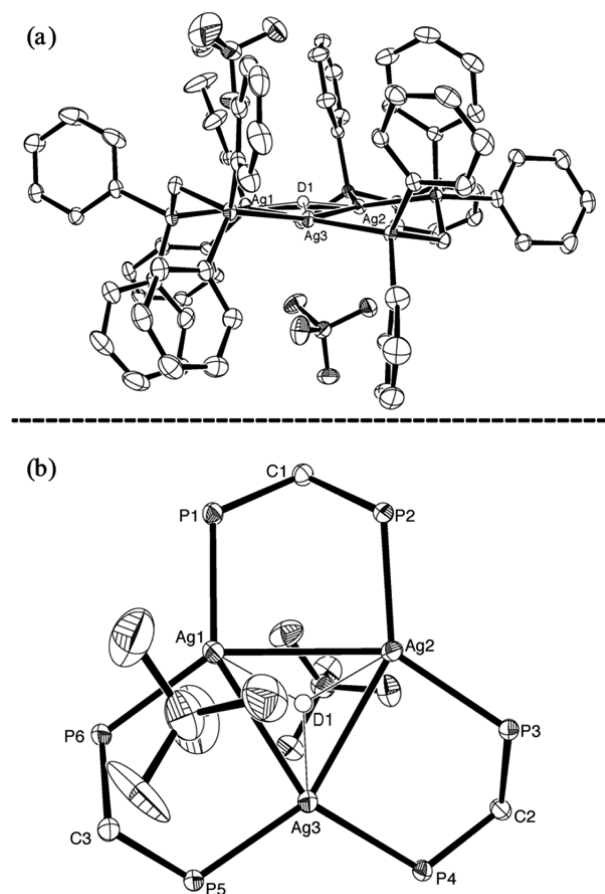
Figure 2. (a) ORTEP-3 representations of **1** with hydrogen atoms and solvent omitted for clarity. (b) Representation of the silver core with the ligand (phenyl rings and hydrogen atoms of the ligand omitted for clarity). Displacement ellipsoids set at the 50% probability level. The location of the deuterium is unambiguously proven by neutron diffraction.

Table 1. Selected Bond Lengths (Å) and Angles (deg) with Estimated Standard Deviations in Parentheses for 1[a]

	distance (Å)	angle (deg)
Ag1–Ag2	3.1511(2)	
Ag1–Ag3	3.1415(2)	
Ag2–Ag3	3.0655(2)	
Ag1–D1	1.85(1)	
Ag2–D1	1.80(1)	
Ag3–D1	1.85(1)	
Ag1–Ag2–Ag3		60.688(4)
Ag2–Ag1–Ag3		58.308(4)
Ag1–Ag3–Ag2		61.004(4)
Ag2–Ag1–D1		32.0(4)
Ag3–Ag1–D1		21.7(4)
Ag3–Ag2–D1		30.3(4)
Ag1–Ag2–D1		33.1(4)
Ag1–Ag3–D1		31.8(4)
Ag2–Ag3–D1		29.5(4)
Ag1–P1	2.4667(5)	
Ag1–P6	2.4769(5)	
Ag2–P2	2.4432(4)	
Ag2–P3	2.4756(4)	
Ag3–P4	2.4596(4)	
Ag3–P5	2.4572(4)	

[a]Distances were determined by X-ray diffraction except those involving deuterium, which were determined by neutron diffraction.

Each cluster can be considered as consisting of three Ag–H/D–Ag–P–C–P six-membered rings sharing adjacent Ag–H/D edges. In turn, the six-membered rings can be assigned a geometric conformation as either a boat or a chair. The $[Ag_3(\mu_3\text{-H/D})L_3]^{2+}$ cation consists of one boat (Ag1–H/D–Ag1–P6–C–P6), with the remaining two in the chair conformation (Scheme 2a). The phosphorus atoms of adjacent ligands at P2 and P3 both have one *pseudo*equatorial phenyl ring with the other pointed toward the hydride/deuteride apex. This allows the vacant site opposite to the hydride apex and toward the *pseudo*equatorial phenyl rings to be occupied by a noncoordinating BF_4^- anion. In contrast, in $[Ag_3(\mu_3\text{-H/D})(Cl)L_3]^+$, the six-membered Ag–H/D–Ag–P–C–P rings all adopt symmetrical chair conformations, and the *pseudo*equatorial phenyl ring at P3 is oriented behind the plane (Scheme 2b). The dihedral angles are shown in Table S1 in the SI, which also compares the dihedral angles of $[Ag_3(\mu_3\text{-H/D})L_3]^{2+}$ to those of $[Ag_3(\mu_3\text{-H/D})(\mu_3\text{-Cl})L_3]^+$.

NMR Spectra of $[Ag_3(\mu_3\text{-H/D})L_3](BF_4)_2$. The most significant feature of the ^{1}H NMR spectrum of **2** (Figure 3) is the multiplet at 4.75 ppm arising from the μ_3-hydride. This resonance integrates as one hydrogen relative to other resonances and displays complex multiplicity. The μ_3-hydride displays coupling to the three silver nuclei of the different isotopomers with further coupling to the six equivalent phosphorus nuclei. This complex multiplet collapses to a broad quartet of quartets in the ^{31}P-decoupled spectrum (Figure 3c and Figure S3 in the SI). It is reassuring that this resonance is absent from the ^{1}H NMR spectrum of **1**, and a broad quartet is present at the same chemical shift in the ^{2}H NMR spectrum of **1** (Figure S9 in the SI).

Simulation of the μ_3-hydride resonance with one-bond coupling constants of 86 and 75 Hz for the coupling of the hydride with ^{109}Ag and ^{107}Ag, respectively, and with a two-bond coupling constant of 21 Hz for the coupling of the hydride with the six equivalent phosphorus nuclei produces a simulated resonance that matches the resonance at 4.75 ppm in the experimental ^{1}H NMR spectrum of **2** (Figure S4a,b in the SI). The simulated pattern is the summation of the individual statistical contributions of the ^{109}Ag$_3$, ^{109}Ag$_2^{107}$Ag, ^{109}Ag^{107}Ag$_2$, and ^{107}Ag$_3$ isotopomers. A simulated ^{31}P-decoupled ^{1}H NMR resonance also correlates well with the 4.75 ppm resonance in the experimental ^{31}P-decoupled NMR spectrum (Figure S4c,d in the SI).

The broad quartet observed at 4.75 ppm in the ^{2}H NMR spectrum of **1** (Figure S9 in the SI) has an apparent coupling constant of 12.4 Hz, being the average of the ^{2}H–^{109}Ag and ^{2}H–^{107}Ag couplings, which are not resolved because of quadrupolar ^{2}H. This average coupling constant scales to an average of 80.7 Hz in the ^{1}H case, which is in good agreement with the observed (simulated) coupling constants of 86 and 75 Hz for the coupling with ^{109}Ag and ^{107}Ag, respectively (Figure S4 in the SI). The expected 3 Hz coupling of the ^{2}H with the ^{31}P nuclei is not resolved.

How does the observed chemical shift of 4.75 ppm for the μ_3-hydride compare to related coinage metal hydride clusters? In the structurally related d^{10} nanocluster, $[Cu_3(\mu_3\text{-H})(dcpm)_3]^{2+}$ [dcpm = bis(dicyclohexylphosphino)methane], a resonance at ∼2.2 ppm was attributed to the hydride because of the fact that it was a septet with $^2J_{P-H}$ = 16 Hz.[19] The chemical

Scheme 2. Representation Highlighting the Contrasting Geometries of the Six-Membered Ag^2-H-P^2-C and Spatial Orientation of the Phenyl Rings for the Cations of (a) $[Ag_3(\mu_3-H/D)L_3](BF_4)_2$ and (b) $[Ag_3(\mu_3-H/D)(\mu_3-Cl)L_3](BF_4)^a$
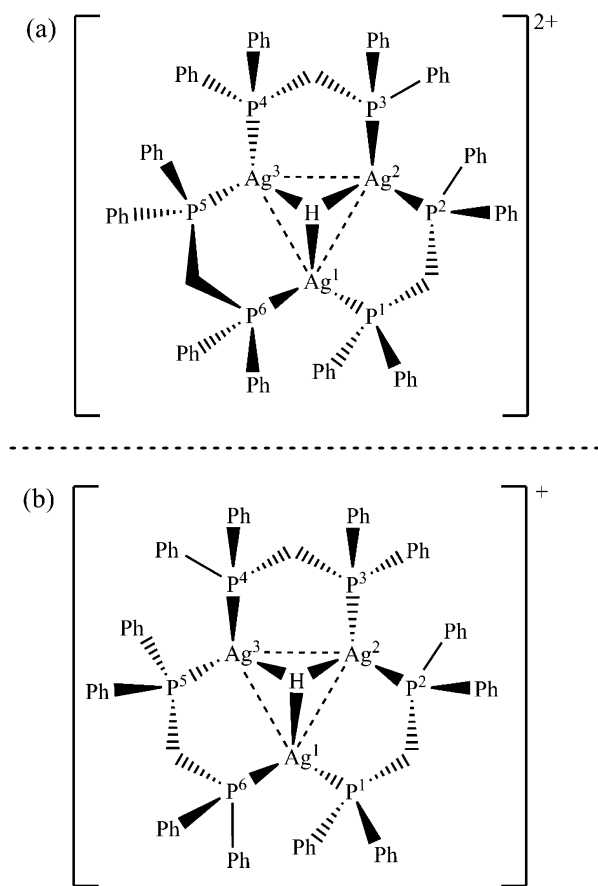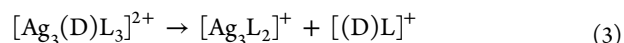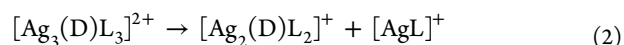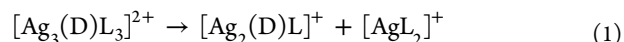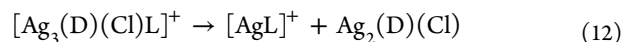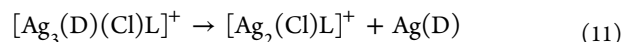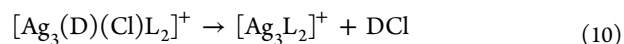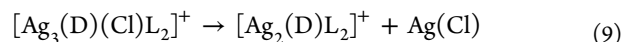

^{a}H represents either the hydride or deuteride.

shifts of the hydrides in the following silver hydride clusters have been reported: (i) $\{[(SIDipp)Ag]_2(\mu-H)\}^+$, triplet of triplets at -1.13 ppm [SIDipp = 1,3-bis(2,6-diisopropylphenyl)imidazolin-2-ylidene];[10d] (ii) $[Ag_7(\mu_4-H)-(Se_2P(O^iPr)_2)_6]$, octet at 3.52 ppm;[10f] (iii) $[Ag_7(\mu_4-H)(S_2P-(OEt)_2)_6]$, octet at 5.65 ppm;[10f] (iv) $[Ag_8(\mu_4-H)(Se_2P-(O^iPr)_2)_6]^+$, nonet at 3.14 ppm;[10b] (v) $[Ag_8(\mu_4-H)(Se_2P-(OEt)_2)_6]^+$, broad multiplet at 3.04 ppm;[10b] (vi) $[Ag_8(\mu_4-H)(S_2P(OEt)_2)_6]^+$, 5.6 ppm;[10a] (vii) $[Ag_{11}(\mu_4-H)-(S_2CNPr_2)_9]^+$, broad multiplet at 7.50 ppm.[10c] Thus, the chemical shift of the hydride is strongly influenced by the capping ligand, cluster nuclearity, and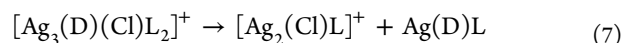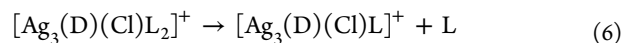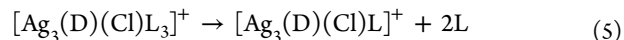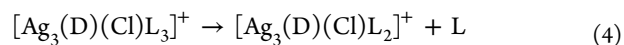 overall charge. Ligands with electron-withdrawing properties result in the chemical shift of the hydride moving downfield, as observed when comparing (iv) $[Ag_8(\mu_4-H)(Se_2P(O^iPr)_2)_6]^+$ with (v) $[Ag_8(\mu_4-H)(Se_2P(OEt)_2)_6]^+$ and (vi) $[Ag_8(\mu_4-H)(S_2P(OEt)_2)_6]^+$, as noted above. The effects of the cluster nuclearity and overall charge are observed when comparing (ii) $[Ag_7(\mu_4-H)(Se_2P-(O^iPr)_2)_6]$ with (iv) $[Ag_8(\mu_4-H)(Se_2P(OEt)_2)_6]^+$ and (iii) $[Ag_7(\mu_4-H)(S_2P(OEt)_2)_6]$ with (vi) $[Ag_8(\mu_4-H)(S_2P-(OEt)_2)_6]^+$.

Unimolecular Gas-Phase Chemistry of $[Ag_3(D)L_3]^{2+}$ and $[Ag_3(D)(BF_4)L_3]^+$ and Comparison to $[Ag_3(D)(Cl)L_3]^+$. Low-energy collision-induced dissociation (CID) has been used

to uncover the lowest-energy fragmentation pathways of coinage metal cluster ions.[12b,c,13] Under these conditions, $[Ag_3(D)L_3]^{2+}$ (m/z 740) fragments via charge-separation reactions including fission of the cluster core (Figure 4a and eqs 1 and 2) and loss of the protonated ligand (Figure 4a and eq 3). The dominant complementary ions observed are $[Ag_2(D)L]^+$ (m/z 602) and $[AgL_2]^+$ (m/z 875) (eq 1). The remaining two charge-separation reactions occur in relatively low abundance (<4%), resulting in formation of the complementary ions (i) $[AgL]^+$ (m/z 491) and $[Ag_2(D)L_2]^+$ (m/z 986) (eq 2) and (ii) $[(D)L]^+$ (m/z 386) and $[Ag_3L_2]^+$ (m/z 1091) (eq 3).

$$[Ag_3(D)L_3]^{2+} \rightarrow [Ag_2(D)L]^+ + [AgL_2]^+ \tag{1}$$

$$[Ag_3(D)L_3]^{2+} \rightarrow [Ag_2(D)L_2]^+ + [AgL]^+ \tag{2}$$

$$[Ag_3(D)L_3]^{2+} \rightarrow [Ag_3L_2]^+ + [(D)L]^+ \tag{3}$$

The unimolecular fragmentation behavior of $[Ag_3(D)L_3]^{2+}$ contrasts with that of $[Ag_3(D)(Cl)L_3]^+$ (Figure S14a in the SI), which exhibits the loss of up to two neutral ligands as the main fragmentation channels (eqs 4 and 5). In addition, $[Ag_3(D)-(Cl)L_3]^+$ also fragments via minor channels (<1%) arising from core fission (eqs 7−9, 11, and 12) and reductive elimination of the core anionic ligands as DCl (eq 10). This latter channel is of interest because it provides a link between ionic and metallic clusters. The differences in the low-energy fragmentation reactions of $[Ag_3(D)L_3]^{2+}$ and $[Ag_3(D)(Cl)L_3]^+$ suggest that the chloride stabilizes the cluster with regard to core fission.

$$[Ag_3(D)(Cl)L_3]^+ \rightarrow [Ag_3(D)(Cl)L_2]^+ + L \tag{4}$$

$$[Ag_3(D)(Cl)L_3]^+ \rightarrow [Ag_3(D)(Cl)L]^+ + 2L \tag{5}$$

$$[Ag_3(D)(Cl)L_2]^+ \rightarrow [Ag_3(D)(Cl)L]^+ + L \tag{6}$$

$$[Ag_3(D)(Cl)L_2]^+ \rightarrow [Ag_2(Cl)L]^+ + Ag(D)L \tag{7}$$

$$[Ag_3(D)(Cl)L_2]^+ \rightarrow [Ag_2(Cl)L_2]^+ + Ag(D) \tag{8}$$

$$[Ag_3(D)(Cl)L_2]^+ \rightarrow [Ag_2(D)L_2]^+ + Ag(Cl) \tag{9}$$

$$[Ag_3(D)(Cl)L_2]^+ \rightarrow [Ag_3L_2]^+ + DCl \tag{10}$$

$$[Ag_3(D)(Cl)L]^+ \rightarrow [Ag_2(Cl)L]^+ + Ag(D) \tag{11}$$

$$[Ag_3(D)(Cl)L]^+ \rightarrow [AgL]^+ + Ag_2(D)(Cl) \tag{12}$$
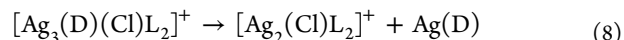
Electron-capture dissociation (ECD)[20] is an activation method different from CID and involves a multiply charged cation interacting with a beam of low-energy electrons. Because ECD has rarely been applied to examine the fragmentation reactions of multiply charged coinage metal clusters,[12c] we were interested in examining the behavior of $[Ag_3(D)L_3]^{2+}$ under ECD conditions (Figure 4b). The 1e$^-$-reduced cluster $[Ag_3(D)L_3]^+$ was not observed, highlighting that, once formed, it spontaneously fragments. Seven different ECD fragmentation pathways were observed (eqs 13−19), including fission of the cluster core (eqs 13−15 and 17), ligand fragmentation via C−P bond activation (eqs 14 and 16), ligand loss (eq 18), and loss of D$^\bullet$ to yield $[Ag_3L_3]^+$ (m/z 1477; eq 19). The major fragmentation channels correspond to the loss of a ligand [L] (eq 18) and the loss of [AgL] (eq 17). The observation of the
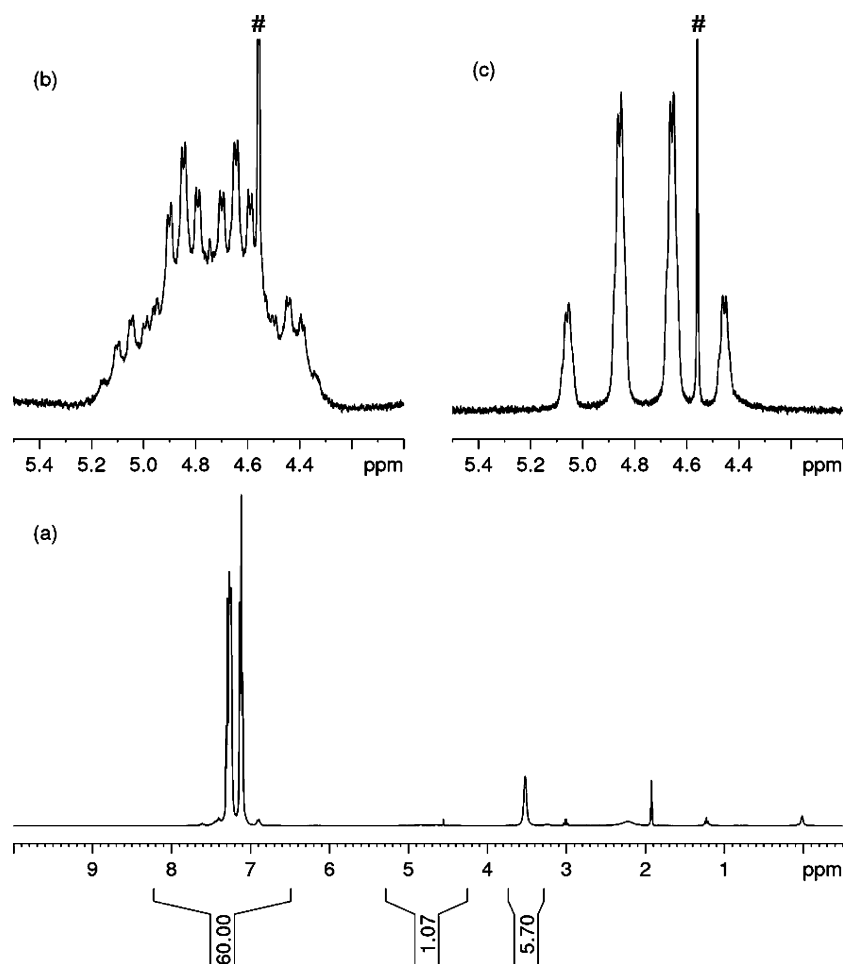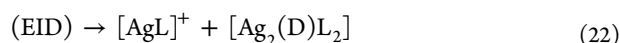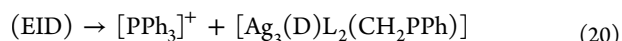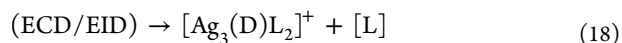
Figure 3. (a) ^{1}H NMR spectrum of $[Ag_3(\mu_3-H)L_3](BF_4)_2$ at 400 MHz in CD_3CN. (b) Expansion of the hydride resonance. (c) Expansion of the hydride resonance taken from the ^{31}P-decoupled ^{1}H NMR spectrum. # indicates the singlet resonance at 4.56 ppm in the experimental spectrum assigned to dissolved H_2.

"all-silver" cluster, $[Ag_3L_3]^+$, is noteworthy because it represents a rare example of a ligated trinuclear silver cation. A related gold nanocluster cation, $[Au_3(SIDipp)_3]^+$, has been isolated and structurally characterized only recently.[21]

$$[Ag_3(D)L_3]^{2+} + e^-$$

$$(ECD/EID) \rightarrow [Ag_2(D)L]^+ + [AgL_2] \tag{13}$$

$$(ECD/EID) \rightarrow [Ag_2L(CH_2PPh_2)]^+ + [Ag(D)L(PPh_2)] \tag{14}$$

$$(ECD/EID) \rightarrow [AgL_2]^+ + [Ag_2(D)L] \tag{15}$$

$$(ECD/EID) \rightarrow [Ag_3(D)L(CH_2PPh_2)]^+ + [L(PPh_2)] \tag{16}$$

$$(ECD/EID) \rightarrow [Ag_2(D)L_2]^+ + [AgL] \tag{17}$$

$$(ECD/EID) \rightarrow [Ag_3(D)L_2]^+ + [L] \tag{18}$$

$$(ECD) \rightarrow [Ag_3L_3]^+ + [D]^\bullet \tag{19}$$

$$(EID) \rightarrow [PPh_3]^+ + [Ag_3(D)L_2(CH_2PPh)] \tag{20}$$

$$(EID) \rightarrow [DL]^+ + [Ag_3L_2] \tag{21}$$

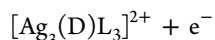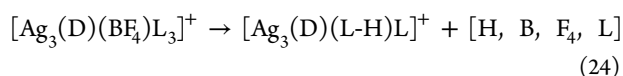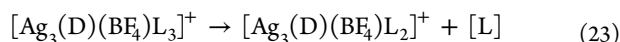$$(EID) \rightarrow [AgL]^+ + [Ag_2(D)L_2] \tag{22}$$
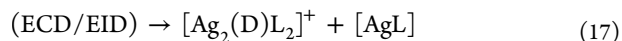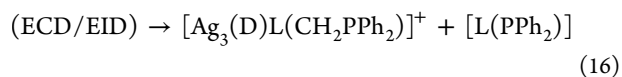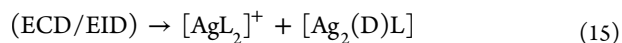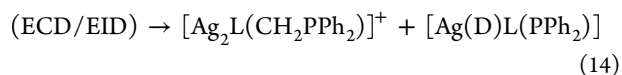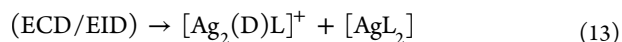
Raising the energy of the electrons (>20 eV) used to activate $[Ag_3(D)L_3]^{2+}$ leads to the electron-induced dissociation (EID) spectrum[20] given in Figure S15 in the SI. While there are some fragment ions that are common to both the ECD and EID spectra (eqs 13–18), $[Ag_3L_3]^+$ is absent in the EID spectrum (eq 19), which also contains the three new fragment ions $[PPh_3]^+$, $[DL]^+$, and $[AgL]^+$, most likely arising via the reactions shown in eqs 20–22.

Our attention then turned to examining the unimolecular chemistry of $[Ag_3(H)(BF_4)L_3]^+$ (m/z 1565; Figure S16 in the SI) and $[Ag_3(D)(BF_4)L_3]^+$ (m/z 1566; Figure 5), which is the deuteride counterpart of the most abundant "postreaction" cluster observed via ESI-MS (Figure 1b). The loss of one ligand (eq 23) and formation of $[Ag_3(D)(BF_4)(L-H)L]^+$ [(L-H) = $(Ph_2P)_2CH^-$; eq 24] are the major fragmentation channels (Figure 5a). Minor channels are observed for the loss of $[Ag(D)L]$ (eq 16) and formation of $[Ag_2(L-H)L]^+$ (eq 26). Note that the product ion $[Ag_2(BF_4)L_2]^+$ (eq 25) is also present in the prereaction spectrum (Figure 1a).

$$[Ag_3(D)(BF_4)L_3]^+ \rightarrow [Ag_3(D)(BF_4)L_2]^+ + [L] \tag{23}$$

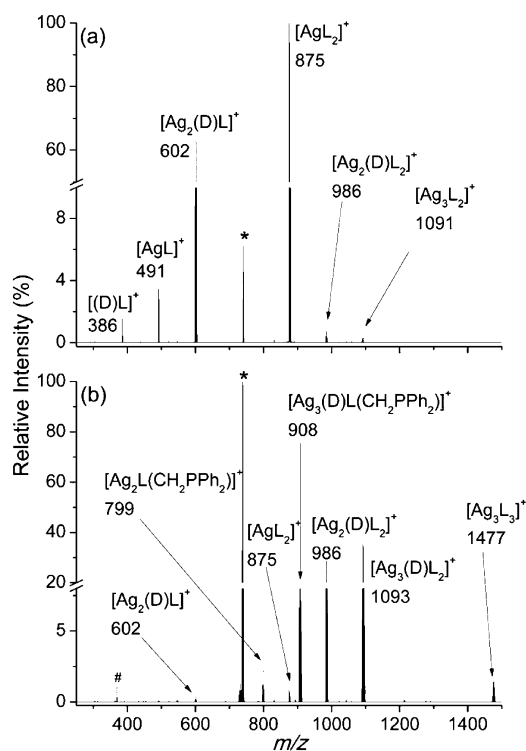$$[Ag_3(D)(BF_4)L_3]^+ \rightarrow [Ag_3(D)(L-H)L]^+ + [H, B, F_4, L] \tag{24}$$

Figure 4. Fragmentation of $[Ag_3(D)L_3]^{2+}$ (m/z 739.5) resulting from (a) CID in the linear ion trap (LIT) and (b) ECD in the FTICR cell at ca. 2 eV. * represents the mass-selected precursor ion $[Ag_3(D)L_3]^{2+}$. # represents a harmonic peak. The most intense isotopic peak of each cluster is represented by the m/z value.

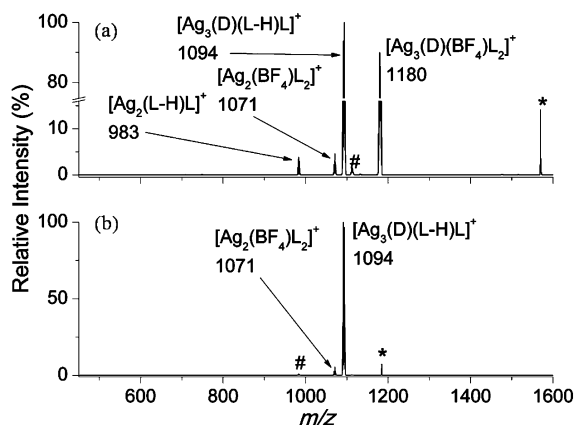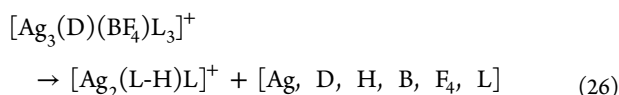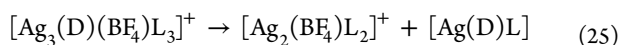**Figure 5.** LTQ CID of $[Ag_3(D)(BF_4)L_n]^+$: (a) n = 3, m/z 1566; (b) n = 2, m/z 1180. The most intense peak in the cluster is represented by the m/z value. * refers to the mass-selected precursor ion. # refers to background water addition.

$$[Ag_3(D)(BF_4)L_3]^+ \rightarrow [Ag_2(BF_4)L_2]^+ + [Ag(D)L] \quad (25)$$

$$[Ag_3(D)(BF_4)L_3]^+$$
$$\rightarrow [Ag_2(L\text{-}H)L]^+ + [Ag, D, H, B, F_4, L] \quad (26)$$

Mass selecting the product ion $[Ag_2(BF_4)L_2]^+$ (m/z 1071) for further CID (eq 27 and Figure S18a in the SI) results in a fragmentation similar to that of $[Ag_3(D)(BF_4)L_3]^+$, where the major fragmentation channel of $[Ag_2(BF_4)L_2]^+$ is due to the loss of the elements of $[H, B, F_4]$ (eq 27), which could

correspond to the combined loss of HF and BF_3, possibly as the $HF \cdot BF_3$ complex.[22] Fragmentation reactions that result in deprotonation of a coordinated dppm ligand were not observed in the CID spectra of $[Ag_3(D)L_3]^{2+}$ or $[Ag_3(D)(Cl)L_3]^+$. It is not clear whether this is due to the fact that decomposition of the tetrafluoroborate anion releases F^-, which is a more potent gas-phase base than Cl^-,[23] or whether it is due to the fact that Cl remains bound to the Ag_3 core in $[Ag_3(D)(Cl)L_3]^+$, while $[Ag_3(D)(BF_4)L_3]^+$ and $[Ag_2(BF_4)L_2]^+$ have contact ion-pair structure(s).

$$[Ag_2(BF_4)L_2]^+ \rightarrow [Ag_2(L\text{-}H)L]^+ + [H, B, F_4] \quad (27)$$
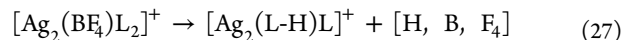
■ CONCLUSIONS

The structural characterization via both neutron and X-ray diffraction, of a small dicationic silver hydride bis(phosphine)-ligated nanocluster, $[Ag_3(\mu_3\text{-}H)(L)_3](BF_4)_2$, formed by the reaction of silver salts with $NaBH_4$ in the presence of a bis(phosphine) ligand, is presented. This cluster augments the small collection of dicationic CMNCs that has been structurally characterized, including $[Cu_3(\mu_3\text{-}H)(dcpm)_3]X_2$ [X = ClO_4^-, BF_4^-, PF_6^-, $CF_3SO_3^-$; dcpm = bis(dicyclohexylphosphino)-methane][19] and $[Ag_3(\mu_3\text{-}CCAr)(dppm)_3](BF_4)_2$ (Ar = Ph, p-$MeOC_6H_5$, p-$O_2NC_6H_5$),[24] and highlights the value of neutron diffraction for the definitive determination of the structures of metal hydrides. In the present example, the addition of borohydride expands the nuclearity of the clusters formed, leading to a silver(I) hydride complex and not a mixed-valent silver(0/I) cluster. This is of particular interest considering the reported preparations of nanoclusters and nanoparticles formed by reactions of silver salts with $NaBH_4$.

A comparison of the gas-phase fragmentation reactions of $[Ag_3(\mu_3\text{-}H)(dppm)_3]^{2+}$ and $[Ag_3(\mu_3\text{-}H)(\mu_3\text{-}Cl)(dppm)_3]^+$ reveals that the chloride stabilizes the cluster with respect to fission of the silver core. ESI-MS is a valuable technique to direct the synthesis of CMNCs, to monitor the molecular nature of their assembly, and to study their reactivity and dynamics in solution. HRMS, which provides accurate mass assignments together with well-resolved isotope envelopes, is emerging as an important technique to facilitate the assignment of molecular formulas of nanoclusters. By using MS to compare the products of the reactions of silver salts with $NaBH_4$ to those formed with sodium borodeuteride, it is possible to identify the number of hydrides present in a nanocluster.[10a−d,25] Current work is underway to examine the reactivity of $[Ag_3(\mu_3\text{-}H)(dppm)_3]^{2+}$ with inorganic and organic substrates and the synthesis and reactions of other CMNCs.

■ EXPERIMENTAL SECTION

Materials. Chemicals from the following suppliers were used without further purification. (i) Aldrich: bis(diphenylphosphino)-methane (dppm, L; 97%), silver(I) tetrafluoroborate ($AgBF_4$; 98%), and sodium borodeuteride ($NaBD_4$; 98% D, 90% CP). (ii) AJAX: sodium borohydride ($NaBH_4$; 97%). (iii) Merck: methanol (AR grade for synthesis and HPLC grade for ESI-MS^n experiments) and acetronitrile (HPLC grade).

All work described here used analytical-reagent-grade chloroform (Merck), which was further purified according to a literature method.[15] In brief, 250 mL of chloroform was washed three times with deionized water to extract the stabilizing agent and dried with K_2CO_3. The solution was then refluxed with $CaSO_4$, distilled, and stored under argon with 4 Å molecular sieves dried by 3−5 rounds of 30 s microwave irradiation. All purification techniques were carried out

(i) in the dark by covering glassware in foil and (ii) under inert conditions using argon.

MS. MS experiments were conducted on a Finnigan hybrid linear quadrupole Fourier transform ion cyclotron resonance (LTQ FTICR) mass spectrometer. The condensed-phase silver cluster samples were typically diluted in methanol to silver concentrations of 50 μM and injected at a flow rate 5 μL·min^{-1} into the Finnigan ESI source. ESI source conditions typically involved needle potentials of 3.2−4.8 kV to give a stable source current of ca. 0.5 μA and a nitrogen sheath gas pressure of 5 arbitrary units. The ion-transfer capillary temperature was set to 250 °C. The tube lens voltage and capillary voltage were both set to ca. 10.0 V. Unimolecular fragmentation studies involved the cation of interest to be mass-selected in the linear ion trap (LIT) by a range of 10−20 m/z units centered at about the middle of the isotopic cluster and subsequently analyzed by CID, ECD, or EID. In CID experiments, the normalized collision energy was set between 10 and 25 arbitrary units to result in the mass-selected precursor ion to be depleted to 10−20% with an activation Q of 0.25 and an activation time of 30 ms. For high-resolution mass analysis and ECD or EID experiments, see elsewhere.[12c]

Synthesis of Silver Clusters for Analysis by MS. Under ambient conditions, a solution of freshly prepared methanol/chloroform (1:1) stock stored under 3 Å molecular sieves was used to dispense 20 mL of solvent to a 50 mL graduated glass measuring cylinder. To a 25 mL Quickfit Erlenmeyer flask equipped with a magnetic stirbar and a Quickfit stopper and covered in foil was added ca. 15 mL of solvent. The magnetic stirbar was set to spin at 500 rpm. dppm (3.8 mg, 0.010 mmol) was dissolved in a 1 mL glass scintillation vial in ca. 1 mL of solvent by brief sonication, and then the solution was added to the 25 mL Erlenmeyer flask; the vial was rinsed with another 1 mL solvent, and the solution was added to ensure that all of the reagent was transferred. Silver(I) tetrafluoroborate (1.9 mg, 0.010 mmol) was added in the same way as the ligand, with the exception that the 1 mL glass scintillation vial was covered in foil and the transfer was made in the dark to minimize light. NaBH$_4$ (0.8 mg, 0.025 mmol) or sodium borodeuteride (0.8 mg, 0.020 mmol) was added in powder form, which resulted in an immediate bubbling with a color change from colorless to pale orange. The remaining 20 mL of solvent was added to the Erlenmeyer flask, and the flask was sealed with a Quickfit stopper until MS analysis was required.

Synthesis of [Ag$_3$(μ_3-D)L$_3$](BF$_4$)$_2$ (1). Silver(I) tetrafluoroborate (35 mg, 0.2 mmol) and dppm (70 mg, 0.2 mmol) were added to a dry Schlenk tube. The Schlenk tube was covered in foil to minimize exposure to ambient light, and a degassed solution of methanol/chloroform (1:1, ca. 5 mL) was added. Within 5 min, the addition of dry sodium borodeuteride (7 mg, 0.2 mmol) resulted in the formation of gas and an immediate change in color from colorless to orange. This orange solution was left to stir at 500 rpm for ca. 30 min. The solution was frozen, layered with dry diethyl ether (ca. 10 mL), and allowed to stand undisturbed for 2 days to yield crystals of **1** (Figure S19 in the SI) of sufficient quality for analysis by X-ray crystallography and neutron diffraction. For large-scale synthesis, to a solution of acetonitrile (50 mL) was added dppm (0.38 g, 1.0 mmol; the mixture was shielded from ambient light by aluminum foil). To this mixture was added silver(I) tetrafluoroborate (0.20 g, 1.0 mmol), resulting in a clear solution. After ca. 5 min, sodium borohydeuteride (17 mg, 0.4 mmol) was added, resulting in a pale-yellow mixture. After ca. 30 min, the mixture was filtered and the solvent removed by evaporation under vacuum to afford a slightly tan-colored powder of [Ag$_3$(D)L$_3$](BF$_4$)$_2$ (0.65 g, 39%). NMR of **1** from the large-scale synthesis resulted in ^{1}H NMR (5:95 CD$_3$CN/CH$_3$CN, 500.1 MHz): δ_H 7.23 (t, J = 8.4 Hz, 12H, H4), 7.07 (m, 24H, H2), 6.99 (t, J = 7.8 Hz, 24H, H3), 3.16 (br s, 6H). ^{2}H NMR (5:95 CD$_3$CN/CH$_3$CN, 76.8 MHz): δ_D 4.75 (m). ^{31}P NMR (5:95 CD$_3$CN/CH$_3$CN, 162.0 MHz): δ_P 1.55 (br s). ^{13}C NMR (5:95 CD$_3$CN/CH$_3$CN, 100.6 MHz): δ_C 133.2 (br, C2), 132.9 (br, C1), 131.4 (C4), 129.6 (C3), 25.6 (br, CH$_2$). ^{19}F NMR (5:95 CD$_3$CN/CH$_3$CN, 376.5 MHz): δ_F −153.2. High-resolution positive ESI-MS. Found (calcd): m/z 739.54311 (739.54428) ([Ag$_3$(H)L$_3$]$^{2+}$).

Synthesis of [Ag$_3$(μ_3-H)L$_3$](BF$_4$)$_2$ (2). To a solution of acetonitrile (50 mL) was added dppm (0.38 g, 1.0 mmol; the mixture was shielded from ambient light by aluminum foil). To this mixture was added silver(I) tetrafluoroborate (0.20 g, 1.0 mmol), resulting in a clear solution. After ca. 5 min, NaBH$_4$ (15 mg, 0.4 mmol) was added, resulting in a pale-yellow mixture. After ca. 30 min, the mixture was filtered and the solvent removed by evaporation under vacuum to afford a slightly tan-colored powder of [Ag$_3$(H)L$_3$](BF$_4$)$_2$ (0.57 g, 35%). NMR of **2** from the large-scale synthesis resulted in ^{1}H NMR (CD$_3$CN, 400.1 MHz): δ_H 7.27 (m, 36H, H2, H4), 7.12 (m, 24H, H3), 4.75 (m, 1H, μ_3-H), 3.52 (br s, 6H, CH$_2$). ^{31}P NMR (CD$_3$CN, 162.0 MHz): δ_P 6.67 (m). ^{13}C NMR (CD$_3$CN, 100.6 MHz): δ_C 133.9 (br, C2), 132.8 (br, C1), 131.9 (C4), 130.0 (C3), 25.5 (br, CH$_2$). ^{19}F NMR (CD$_3$CN, 376.5 MHz): δ_F −153.3. High-resolution positive ESI-MS. Found (calcd): m/z 739.04139 (739.04114) ([Ag$_3$(H)L$_3$]$^{2+}$).

Laue Neutron Diffraction. The Laue neutron diffraction study was undertaken using the KOALA[26a] diffractometer located on a thermal neutron guide at the OPAL reactor, Australian Nuclear Science and Technology Organization. A total of 26 images each with an exposure time of 10000 s per frame were employed in a data reduction[26b] for diffraction spots with wavelength (λ) in the range 0.85−1.70 Å, yielding 64498 reflections, of which 5994 were unique and 4647 met the 3σ criterion of observability. Structure refinement[26c] commenced from the X-ray-determined structure for which a scale factor and isotropic displacement parameters were derived and then all H/D atomic sites were deleted from the model. A difference density map revealed the position of all hydrogen atoms of the complex cluster cation as negative features, and the position of the deuterium was similarly evident as a positive feature. Positional and isotropic displacement parameters for all atoms were included in the initial full-matrix least-squares refinement, and anisotropic modeling could only be extended to include the silver, boron, and fluorine atoms plus the carbon of the solvating methanol; further extension of modeling (the addition of more parameters) yielded ill-conditioned matrices and unstable refinements.

Crystallographic Data and Structure Refinement for 1: C$_{75}$H$_{66}$D$_1$Ag$_3$B$_2$F$_8$P$_6$·0.5CH$_3$OH, M = 1668.43, T = 130.0(2) K, monoclinic, space group $I2/a$, a = 26.9665(10) Å, b = 13.2190(4) Å, c = 39.5373(8) Å, β = 96.589(2)°, V = 14000.8(7) Å^3, Z = 8, D_c = 1.582 Mg·m^{-3}.

X-ray: T = 130 K, F(000), 6712, μ(Mo Kα) = 1.034 mm^{-1}, λ = 0.71069 Å, crystal size 0.55 × 0.36 × 0.25 mm. 73424 reflections measured, 27244 independent reflections (R_{int} = 0.0260), 890 parameters, the final R was 0.0318 [$I > 3\sigma(I)$] and $R_w(F^2)$ (all data) was 0.0691.

Laue neutron: T = 123 K, F(000) = 2980, crystal size 0.8 × 1.0 × 2.0 mm, 64498 reflections measured, 5994 independent reflections [merging R = 13(8)%], 4647 data [$I > 3\sigma(I)$] used in refinement the final R was 0.128 and R_w = 0.1051 for 723 parameters.

NMR Spectroscopy. NMR experiments were performed on a Bruker Avance 500 NMR spectrometer (500.13 MHz ^{1}H frequency) equipped with a 5 mm inverse triple resonance (^{1}H/^{2}H−^{13}C/^{15}N) probe or a Bruker Avance 400 NMR spectrometer (400.13 MHz ^{1}H frequency) equipped with a 5 mm triple resonance broad-band probe (BB/^{2}H−^{1}H/^{19}F). Samples were maintained at a regulated 25 °C inside the probe. Chemical shifts were referenced to the residual protonated solvent peak ^{1}H (CD$_2$HCN, 1.94 ppm), the solvent peak ^{13}C (CD$_3$CN, 1.39 ppm), the solvent peak ^{2}H (CD$_3$CN, 1.94 ppm), or external CFCl$_3$ in CDCl$_3$ (^{19}F, 0.00 ppm) or 85% H$_3$PO$_4$ (^{31}P, 0.00 ppm). NMR samples were prepared by dissolving 90−100 mg of [Ag$_3$(H)L$_3$](BF$_4$)$_2$ in 0.6 mL of deuterioacetonitrile or [Ag$_3$(D)L$_3$]-(BF$_4$)$_2$ in 0.6 mL of 5:95 deuterioacetonitrile/acetonitrile.

^{1}H NMR spectra were acquired using a 30° acquisition pulse and a total recycle delay of ca. 4 s. ^{31}P decoupling of ^{1}H NMR spectra was achieved using the garp4 sequence. ^{2}H NMR spectra were acquired without ^{2}H lock using a 90° acquisition pulse and a total recycle delay of ca. 6 s. ^{13}C, ^{19}F, and ^{31}P NMR spectra were all ^{1}H-decoupled using the waltz65 sequence; ^{19}F and ^{31}P experiments used inverse-gated decoupling.

Simulations of NMR spectra were performed using *NMR-SIM* 5.5.3 (Kessler, P., Bruker BioSpin GmbH, Rheinstetten, Germany, 2014).

■ ASSOCIATED CONTENT

S Supporting Information

Full citation of ref 18f, mass spectra, spectroscopic characterization, figures and bond angles, and results of crystallographic studies in CIF format. This material is available free of charge via the Internet at http://pubs.acs.org. The CIF files have also been deposited with the Cambridge Crystallographic Data Centre as CCDC 978349 (X-ray) and 978350 (neutron). The coordinates can be obtained, upon request, from the Director, Cambridge Crystallographic Data Centre, 12 Union Road, Cambridge CB2 1EZ, U.K.

■ AUTHOR INFORMATION

Corresponding Authors
*E-mail: gkhai@unimelb.edu.au. Fax: (+) 61 3 9347 8124.
*E-mail: pauld@unimelb.edu.au. Fax: (+) 61 3 9347 8124.
*E-mail: rohair@unimelb.edu.au. Fax: (+) 61 3 9347 8124.

Notes
The authors declare no competing financial interest.

■ ACKNOWLEDGMENTS

■ REFERENCES

(1) (a) Daniel, M.-C.; Astruc, D. *Chem. Rev.* **2003**, *104* (1), 293−346. (b) Rao, C. N. R.; Kulkarni, G. U.; Thomas, P. J.; Edwards, P. P. *Chem. Soc. Rev.* **2000**, *29* (1), 27−35. (c) Wilcoxon, J. P.; Abrams, B. L. *Chem. Soc. Rev.* **2006**, *35* (11), 1162−1194. (d) Jin, R. *Nanoscale* **2010**, *2* (3), 343−362. (e) Guo, S.; Wang, E. *Nano Today* **2011**, *6* (3), 240−264. (f) Lu, Y.; Chen, W. *Chem. Soc. Rev.* **2012**, *41* (9), 3594−3623. (g) Yau, S. H.; Varnavski, O.; Goodson, T. *Acc. Chem. Res.* **2013**, *46* (7), 1506−1516. (h) Udayabhaskararao, T.; Pradeep, T. *J. Phys. Chem. Lett.* **2013**, *4* (9), 1553−1564. (i) Zhao, P.; Li, N.; Astruc, D. *Coord. Chem. Rev.* **2013**, *257* (3−4), 638−665.

(2) (a) Haruta, M.; Yamada, N.; Kobayashi, T.; Iijima, S. *J. Catal.* **1989**, *115* (2), 301−309. (b) Haruta, M. *Catal. Today* **1997**, *36* (1), 153−166. (c) Bond, G. C.; Thompson, D. T. *Catal. Rev.: Sci. Eng.* **1999**, *41* (3−4), 319−388. (d) Haruta, M. *Chem. Rec.* **2003**, *3* (2), 75−87.

(3) (a) Zharov, V. P.; Kim, J.-W.; Curiel, D. T.; Everts, M. *Nano. Nano. Biol. Med.* **2005**, *1* (4), 326−345. (b) Canelas, D. A.; Herlihy, K. P.; DeSimone, J. M. *Nanomed. Nanobiotechnol.* **2009**, *1* (4), 391−404. (c) Debbage, P.; Jaschke, W. *Histochem. Cell Biol.* **2008**, *130* (5), 845−875. (d) Tam, J. M.; Tam, J. O.; Murthy, A.; Ingram, D. R.; Ma, L. L.; Travis, K.; Johnston, K. P.; Sokolov, K. V. *ACS Nano* **2010**, *4* (4), 2178−2184.

(4) (a) Peyser, L. A.; Vinson, A. E.; Bartko, A. P.; Dickson, R. M. *Science* **2001**, *291* (5501), 103−106. (b) Liz-Marzán, L. M. *Langmuir* **2005**, *22* (1), 32−41. (c) Kneipp, K.; Kneipp, H.; Kneipp, J. *Acc. Chem. Res.* **2006**, *39* (7), 443−450.

(5) (a) Bertino, M. F.; Sun, Z. M.; Zhang, R.; Wang, L. S. *J. Phys. Chem. B* **2006**, *110* (43), 21416−21418. (b) Bergeron, D. E.; Hudgens, J. W. *J. Phys. Chem. C* **2007**, *111* (23), 8195−8201. (c) Golightly, J. S.; Gao, L.; Castleman, A. W., Jr.; Bergeron, D. E.; Hudgens, J. W.; Magyar, R. J.; Gonzalez, C. A. *J. Phys. Chem. C* **2007**, *111* (40), 14625−14627. (d) Bergeron, D. E.; Coskuner, O.; Hudgens, J. W.; Gonzalez, C. A. *J. Phys. Chem. C* **2008**, *112* (33), 12808−12814. (e) Pettibone, J. M.; Hudgens, J. W. *J. Phys. Chem. Lett.* **2010**, *1* (17), 2536−2540. (f) Shichibu, Y.; Konishi, K. *Small* **2010**, *6* (11), 1216−1220. (g) Pettibone, J. M.; Hudgens, J. W. *ACS Nano* **2011**, *5* (4),

2989−3002. (h) Hudgens, J. W.; Pettibone, J. M.; Senftle, T. P.; Bratton, R. N. *Inorg. Chem.* **2011**, *50* (20), 10178−10189. (i) Pettibone, J. M.; Hudgens, J. W. *Phys. Chem. Chem. Phys.* **2012**, *14* (12), 4142−4154. (j) Pettibone, J. M.; Hudgens, J. W. *Small* **2012**, *8* (5), 715−725. (k) Shichibu, Y.; Suzuki, K.; Konishi, K. *Nanoscale* **2012**, *4* (14), 4125−4129.

(6) (a) Ingram, R. S.; Hostetler, M. J.; Murray, R. W.; Schaaff, T. G.; Khoury, J. T.; Whetten, R. L.; Bigioni, T. P.; Guthrie, D. K.; First, P. N. *J. Am. Chem. Soc.* **1997**, *119* (39), 9279−9280. (b) Chen, S.; Ingram, R. S.; Hostetler, M. J.; Pietron, J. J.; Murray, R. W.; Schaaff, T. G.; Khoury, J. T.; Alvarez, M. M.; Whetten, R. L. *Science* **1998**, *280* (5372), 2098−2101. (c) Schaaff, T. G.; Shafigullin, M. N.; Khoury, J. T.; Vezmar, I.; Whetten, R. L.; Cullen, W. G.; First, P. N.; Gutiérrez-Wing, C.; Ascensio, J.; Jose-Yacamán, M. J. *J. Phys. Chem. B* **1997**, *101* (40), 7885−7891.

(7) (a) Tang, Y.; Ouyang, M. *Nat. Mater.* **2007**, *6* (10), 754−759. (b) Zheng, N.; Fan, J.; Stucky, G. D. *J. Am. Chem. Soc.* **2006**, *128* (20), 6550−6551. (c) Peng, S.; McMahon, J. M.; Schatz, G. C.; Gray, S. K.; Sun, Y. *Proc. Natl. Acad. Sci. U.S.A.* **2010**, *107* (33), 14530−14534. (d) Jana, N. R.; Peng, X. *J. Am. Chem. Soc.* **2003**, *125* (47), 14280−14281.

(8) (a) Yang, H.; Lei, J.; Wu, B.; Wang, Y.; Zhou, M.; Xia, A.; Zheng, L.; Zheng, N. *Chem. Commun.* **2013**, *49*, 300−302. (b) Yang, H.; Wang, Y.; Zheng, N. *Nanoscale* **2013**, *5* (7), 2674−2677.

(9) (a) Yang, H.; Wang, Y.; Huang, H.; Gell, L.; Lehtovaara, L.; Malola, S.; Häkkinen, H.; Zheng, N. *Nat. Commun.* **2013**, *4*, 2422. (b) Desireddy, A.; Conn, B. E.; Guo, J.; Yoon, B.; Barnett, R. N.; Monahan, B. M.; Kirschbaum, K.; Griffith, W. P.; Whetten, R. L.; Landman, U.; Bigioni, T. P. *Nature* **2013**, *501*, 399−402.

(10) (a) Liu, C. W.; Chang, H. W.; Fang, C. S.; Sarkar, B.; Wang, J. C. *Chem. Commun.* **2010**, *46* (25), 4571−4573. (b) Liu, C. W.; Chang, H.-W.; Sarkar, B.; Saillard, J.-Y.; Kahlal, S.; Wu, Y.-Y. *Inorg. Chem.* **2010**, *49* (2), 468−475. (c) Liu, C. W.; Liao, P.-K.; Fang, C.-S.; Saillard, J.-Y.; Kahlal, S.; Wang, J.-C. *Chem. Commun.* **2011**, *47* (20), 5831−5833. (d) Tate, B. K.; Wyss, C. M.; Bacsa, J.; Kluge, K.; Gelbaum, L.; Sadighi, J. P. *Chem. Sci.* **2013**, *4* (8), 3068−3074. (e) Latouche, C.; Kahlal, S.; Lin, Y. R.; Liao, J. H.; Furet, E.; Liu, C. W.; Saillard, J.-Y. *Inorg. Chem.* **2013**, *52* (22), 7752−7765. (f) Liu, C. W.; Lin, Y.; Fang, C. S.; Latouche, C.; Kahlal, S.; Saillard, J.-Y. *Inorg. Chem.* **2013**, *52* (4), 2070−2077.

(11) For gas-phase studies of bare silver hydride clusters, see: (a) Khairallah, G. N.; O'Hair, R. A. J. *Angew. Chem., Int. Ed.* **2005**, *44* (5), 728−731. (b) Khairallah, G. N.; O'Hair, R. A. J. *Dalton Trans.* **2005**, *16*, 2702−2712. (c) Khairallah, G. N.; O'Hair, R. A. J. *Dalton Trans.* **2007**, *29*, 3149−3157. (d) Khairallah, G. N.; O'Hair, R. A. J. *Dalton Trans.* **2008**, *22*, 2956−2965. (e) Wang, F. Q.; Khairallah, G. N.; O'Hair, R. A. J. *Int. J. Mass Spectrom.* **2009**, *283* (1−3), 17−25. (f) Donald, W. A.; O'Hair, R. A. J. *Dalton Trans.* **2012**, *41* (11), 3185−3193.

(12) (a) Robinson, P. S. D.; Khairallah, G. N.; Da Silva, G.; Lioe, H.; O'Hair, R. A. J. *Angew. Chem., Int. Ed.* **2012**, *51* (16), 3812−3817. (b) Robinson, P. S. D.; Nguyen, T. L.; Lioe, H.; O'Hair, R. A. J.; Khairallah, G. N. *Int. J. Mass Spectrom.* **2012**, *330−332*, 109−117. (c) Zavras, A.; Khairallah, G. N.; O'Hair, R. A. J. *Int. J. Mass Spectrom.* **2013**, *354−355* (0), 242−248.

(13) Zavras, A.; Khairallah, G. N.; Connell, T. U.; White, J. M.; Edwards, A. J.; Donnelly, P. S.; O'Hair, R. A. J. *Angew. Chem., Int. Ed.* **2013**, *52* (32), 8391−8394.

(14) (a) Franzoni, D.; Pelizzi, G.; Predieri, G.; Tarasconi, P.; Vitali, F.; Pelizzi, C. *J. Chem. Soc., Dalton Trans.* **1989**, *2*, 247−252. (b) Zhou, W.-B.; Dong, Z.-C.; Song, J.-L.; Zeng, H.-Y.; Cao, R.; Guo, G.-C.; Huang, J.-S.; Li, J. *J. Cluster Sci.* **2002**, *13* (1), 119−136. (c) Di Nicola, C.; Effendy; Fazaroh, F.; Pettinari, C.; Skelton, B. W.; Somers, N.; White, A. H. *Inorg. Chim. Acta* **2005**, *358* (3), 720−734.

(15) Armarego, W. L. F.; Perrin, D. D. *Purification of laboratory chemicals*, 4th ed.; Butterworth-Heinemann: Boston, MA, 1996.

(16) (a) Ahrens, B.; Jones, P. G. *Acta Crystallogr.* **1998**, *54* (1), 16−18. (b) Wei, Q.; Yin, G.; Chen, Z. *Acta Crystallogr., Sect. E* **2003**, *59* (5), m232−m233. (c) Ho, D. M.; Bau, R. *Inorg. Chem.* **1983**, *22* (26),

4073−4079. (d) For a comprehensive review of the coordination chemistry of silver(I) with phosphine-containing ligands, see: Meijboom, R.; Bowen, R. J.; Berners-Price, S. J. *Coord. Chem. Rev.* **2009**, *253* (3−4), 325−342.

(17) (a) Allen, F. H. *Acta Crystallogr.* **2002**, *B58*, 380−388. (b) For a review of metal complexes containing weakly coordinating anions such as BF_4^-, see: Beck, W.; Suenkel, K. *Chem. Rev.* **1988**, *88*, 1405−1421.

(18) The chemical shift of the resonance attributed to the μ_3-hydride in $[Ag_3L_3(\mu_3\text{-H})](BF_4)_2$ was predicted to be +2.9 ppm using the gauge atomic orbital (GIAO) method: (a) London, F. *J. Phys. Radium* **1937**, *8*, 397−409. (b) McWeeny, R. *Phys. Rev.* **1962**, *126* (3), 1028−1034. (c) Ditchfield, R. *Mol. Phys.* **1974**, *27* (4), 789−807. (d) Dodds, J. L.; McWeeny, R.; Sadlej, A. J. *Mol. Phys.* **1977**, *34* (6), 1779−1791. (e) Wolinski, K.; Hinton, J. F.; Pulay, P. *J. Am. Chem. Soc.* **1990**, *112* (23), 8251−8260. The *Gaussian 09* software package was used for these GIAO calculations: (f) Frisch, M. J.; et al. *Gaussian 09*, revision B.01; Gaussian Inc.: Wallingford, CT, 2009.

(19) Mao, Z.; Huang, J. S.; Che, C. M.; Zhu, N.; Leung, S. K. Y.; Zhou, Z. Y. *J. Am. Chem. Soc.* **2005**, *127* (13), 4562−4563.

(20) Feketeova, L.; Khairallah, G. N.; O'Hair, R. A. J. *Eur. J. Mass Spectrom.* **2008**, *14* (2), 107−110.

(21) Robilotto, T. J.; Bacsa, J.; Gray, T. G.; Sadighi, J. P. *Angew. Chem., Int. Ed.* **2012**, *51* (48), 12077−12080.

(22) In the gas phase, tetrafluoroboric acid exists as a weakly bound complex between HF and BF_3: (a) Phillips, J. A.; Canagaratna, M.; Goodfriend, H.; Grushow, A.; Almlof, J.; Leopold, K. R. *J. Am. Chem. Soc.* **1995**, *117*, 12549−12556. (b) Nauta, K.; Miller, R. E.; Fraser, G. T.; Lafferty, W. J. *Chem. Phys. Lett.* **2000**, *322* (5), 401−406. (c) Heidrich, D. *Phys. Chem. Commun.* **1999**, *2*, 62−66.

(23) Hunter, E. P. L.; Lias, S. G. *J. Phys. Chem. Ref. Data* **1998**, *27* (3), 413−656.

(24) Yam, V. W.-W.; Fung, W. K.-M.; Cheung, K.-K. *Organometallics* **1997**, *16* (10), 2032−2037.

(25) This is reminiscent of the use of H/D exchange in mass spectrometry experiments to identify the number of exchangeable protons. See: Lam, W.; Ramanathan, R. *J. Am. Soc. Mass Spectrom.* **2002**, *13* (4), 345−353 and references cited therein.

(26) (a) Edwards, A. J. *Aust. J. Chem.* **2011**, *64*, 869−872. (b) Piltz, R. *Acta Crystallogr., Sect. A* **2011**, *67*, C155. (c) Betteridge, P. W.; Carruthers, J. R.; Cooper, R. I.; Prout, K.; Watkin, D. J. *J. Appl. Crystallogr.* **2003**, *36*, 1487.